Atmos. Chem. Phys., 11, 4491–4503, 2011
www.atmos-chem-phys.net/11/4491/2011/
doi:10.5194/acp-11-4491-2011

Atmospheric Chemistry and Physics

Estimate of bias in Aura TES HDO/H_2O profiles from comparison of TES and in situ HDO/H_2O measurements at the Mauna Loa observatory

J. Worden[1], **D. Noone**[2], **J. Galewsky**[3], **A. Bailey**[2], **K. Bowman**[1], **D. Brown**[2], **J. Hurley**[3], **S. Kulawik**[1], **J. Lee**[1], **and M. Strong**[3]

[1]Jet Propulsion Laboratory/California Institute of Technology, Pasadena, California, USA
[2]University of Colorado, CIRES Boulder, Colorado, USA
[3]University of New Mexico, Dept. of Earth and Planetary Sciences, Albuquerque, New Mexico, USA

Received: 4 October 2010 – Published in Atmos. Chem. Phys. Discuss.: 1 November 2010
Revised: 18 April 2011 – Accepted: 18 April 2011 – Published: 12 May 2011

Abstract. The Aura satellite Tropospheric Emission Spectrometer (TES) instrument is capable of measuring the HDO/H_2O ratio in the lower troposphere using thermal infrared radiances between 1200 and 1350 cm^{-1}. However, direct validation of these measurements is challenging due to a lack of in situ measured vertical profiles of the HDO/H_2O ratio that are spatially and temporally co-located with the TES observations. From 11 October through 5 November 2008, we undertook a campaign to measure HDO and H_2O at the Mauna Loa observatory in Hawaii for comparison with TES observations. The Mauna Loa observatory is situated at 3.1 km above sea level or approximately 680 hPa, which is approximately the altitude where the TES HDO/H_2O observations show the most sensitivity. Another advantage of comparing in situ data from this site to estimates derived from thermal IR radiances is that the volcanic rock is heated by sunlight during the day, thus providing significant thermal contrast between the surface and atmosphere; this thermal contrast increases the sensitivity to near surface estimates of tropospheric trace gases. The objective of this intercomparison is to better characterize a bias in the TES HDO data, which had been previously estimated to be approximately 5 % too high for a column integrated value between 850 hPa and 500 hPa. We estimate that the TES HDO profiles should be corrected downwards by approximately 4.8 % and 6.3 % for Versions 3 and 4 of the data respectively. These corrections must account for the vertical sensitivity of the TES HDO estimates. We estimate that the precision of this bias correction is approximately 1.9 %. The accuracy is driven by the corrections applied to the in situ HDO and H_2O measurements using flask data taken during the inter-comparison campaign and is estimated to be less than 1 %. Future comparisons of TES data to accurate vertical profiles of in situ measurements are needed to refine this bias estimate.

Correspondence to: J. Worden
(john.worden@jpl.nasa.gov)

1 Introduction

Measurements of the isotopic composition of water vapor are useful for understanding the distribution of sources, sinks, and processes affecting water because the isotopic composition of water vapor is sensitive to phase changes and also to the isotopic ratio, or "fingerprint", of the original moisture source (e.g. Craig, 1961; Dansgaard, 1964). Satellite measurements of the isotopic composition of water vapor have provided insights into the sources of water into the upper troposphere and lower stratosphere (e.g., Moyer et al., 1996; Kuang et al., 2003; Nassar et al., 2007; Payne et al., 2007; Steinwagner et al., 2010) and more recently for characterizing the distribution of hydrological processes in the free troposphere (e.g., Zakharov et al., 2004; Herbin et al., 2009; J. Worden et al., 2006, 2007; Brown et al., 2008; Frankenberg et al., 2009; Galewsky et al., 2007).

However, very few direct validations of these satellite measurements exist because of the difficulty in obtaining vertical profiles of the isotopic composition of water vapor that

are co-located with satellite data. Most validations of these data have therefore relied on indirect comparisons of the distributions of water vapor isotopes between satellite and aircraft (e.g. Webster and Heymsfield, 2003) or validation of the H_2O measurements, which in turn can be used to assess the errors on the estimate of the HDO/H_2O ratio (e.g., Worden et al., 2006; Herbin et al., 2007, 2009). There are several currently operational sounders measuring the isotopic composition of water vapor such as the Tropospheric Emission Spectrometer (TES), the Atmospheric Chemistry Experiment (ACE), the Infrared Atmospheric Sounding Interferometer (IASI), the SCanning Imaging Absorption SpectroMeter for Atmospheric CHartographY (SCIAMACHY), and the Greenhouse gases Observing SATellite (GOSAT), as well as several future satellites such as the IASI 2 and the Tropospheric Ozone Monitoring Instrument (TropOMI, http://www.knmi.nl/samenw/tropomi/) that plan on measuring the isotopic composition of water vapor. In addition, the application of these measurements for assessing tropospheric and stratospheric moisture sources (evaporation), sinks (rain), cloud processes, and mixing processes is rapidly growing (e.g., J. Worden et al., 2007; Brown et al., 2008; Risi et al., 2008; Frankenberg et al., 2009; Lee et al., 2009; Galewsky et al., 2007). As a consequence there is a need for more robustly assessing the biases as well as the theoretical versus random errors in these data (e.g., Boxe et al., 2010), especially for the lower tropospheric/boundary layer measurements where random errors in the satellite data can be as large or larger than the variability observed in the HDO/H_2O ratio using in situ measurements (e.g., Frankenberg et al., 2009).

Two new approaches for validation of satellite based tropospheric measurements of water vapor and its isotopes are now available. One relies on upward looking solar occultation measurements that can estimate vertical profiles of HDO and H_2O with approximately 1.5–2 degrees-of-freedom for signal (DOFS) (Schneider et al., 2006; Frankenberg et al., 2009); we do not use this approach in this study as it requires a targeted set of measurements from the TES satellite that have yet to be implemented. In this paper we describe the results of an inter-comparison campaign from 8 October through 5 November 2008 in which high speed in situ measurements of water vapor and its isotopes were taken at the Mauna Loa observatory and compared to targeted observations from the Aura TES instrument. This inter-comparison approach was developed because the vertical sensitivity of the TES HDO/H_2O ratio peaks at approximately 700 hPa, which is close to the altitude of Mauna Loa (3.1 km, 680 hPa).

Two types of comparisons are made: (1) satellite observed distributions, within 1000 km of Mauna Loa, of the TES HDO/H_2O relative to H_2O are compared against this same distribution of measurements from Mauna Loa. The distribution is obtained from a campaign in which the TES instrument was directed to take several augmenting observations over the entire north Pacific Ocean (Step-and-Stare Mode); these observations are in addition to its nominal observations that are taken over the whole globe every other day (the TES Global Survey mode). (2) The observations from directly targeting the TES instrument at the Mauna Loa observatory are directly compared to the in situ data. Vertical information of HDO and H_2O are inferred from the in situ measurements by using the diurnal altitude variability of the planetary boundary layer to map in situ measurements of HDO and H_2O to profiles of HDO and H_2O. This altitude distribution is then compared to the TES HDO/H_2O estimates by passing the constructed profile through the TES "instrument operator", which is a function of the observation averaging kernel and an a priori constraint (e.g., H. M. Worden et al., 2007).

2 Data

2.1 In situ measurements

The NOAA Mauna Loa Observatory site is difficult for in situ sampling of water vapor isotopes because it typically sits above the subtropical PBL where the air can be very dry (e.g., Webster and Heymsfield, 2003). Consequently we used a number of measurement approaches for cross-comparison with each other in addition to comparisons with TES. These included a cavity ringdown spectrometer (CRDS) from Picarro (http://www.picarro.com/) (Gupta et al., 2009) and an off-axis integrated cavity output spectrometer (ICOS) from Los Gatos Research (LGR) (http://www.lgrinc.com/) (Lis et al., 2008). The LGR and Picarro data have been corrected using in situ flask measurements taken at Mauna Loa during the TES overpasses as discussed in Johnson et al. (2011). An average of the corrected high speed data are shown in Fig. 1 as a function of the day of year relative to Universal Time (UTC). We expect the accuracy of the corrected in situ data to be approximately 1 %.

2.2 TES data

As discussed in Beer et al. (2001) and Worden et al. (2004), the Tropospheric Emission Spectrometer is an infrared Fourier transform spectrometer (FTS) that measures the spectral infrared (IR) radiances between 650 cm^{-1} and 3050 cm^{-1} in a limb-viewing and a nadir (downward-looking) mode. The observed IR radiance is imaged onto an array of sixteen detectors that have a combined horizontal footprint of 5.3 km by 8.4 km in the nadir viewing mode. In the nadir view, TES estimates of atmospheric distributions provide vertical information of the more abundant tropospheric species such as H_2O, HDO, O_3, CO, and CH_4 (e.g., Worden et al., 2004). However, sufficient spectral resolution and signal-to-noise ratio are required to distinguish between trace-gas amounts at different altitudes because vertical information about trace gas concentrations is obtained only from spectral variations along the line-of-sight. Consequently, the TES spectral resolution was chosen to match the

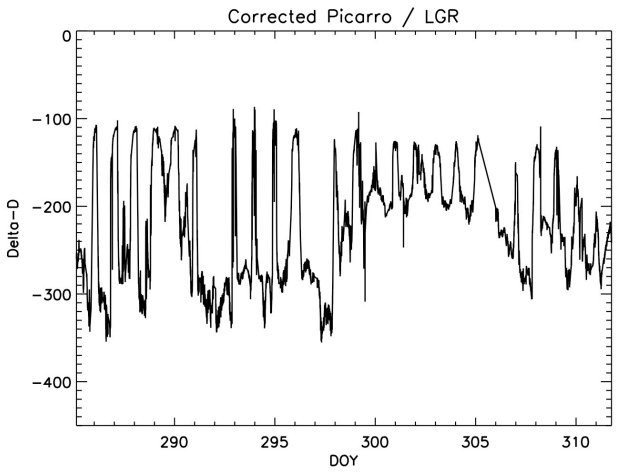

Fig. 1. Corrected time-series from an average of the Picarro/LGR data sets as described in Johnson et al. (2011).

average pressure-broadened widths of weak infrared molecular transitions in the lower troposphere for nadir measurements (0.06 cm^{-1} apodized) (Beer et al., 2001).

The vertical resolution and error characteristics for the HDO/H_2O estimates from TES are discussed in Worden et al. (2006). Briefly, under clear-sky conditions in the tropics, TES estimates of the HDO/H_2O ratio are sensitive to the distribution of the actual ratio from the surface ($\sim$1000 hPa) to about 300 hPa with peak sensitivity at 700 hPa. The sensitivity decreases with latitude through its dependence on temperature and water amount. We estimate a precision of approximately 1 % to 2 % for the TES estimate of the HDO/H_2O ratio. In addition, Worden et al. (2006) estimated that there was a bias of approximately 5 % for column averaged HDO/H_2O estimates between 850 and 500 hPa, where the TES HDO estimates are typically most sensitive by comparing distributions of the TES data to models and aircraft.

3 Bias correction to HDO/H_2O ratio

Worden et al. (2006) found that the TES HDO/H_2O ratios in the Version 3 data were likely biased by approximately 5–6 % by comparing distributions of the HDO/H_2O ratio with model and aircraft data. Our primary objective of the Mauna Loa validation experiment is to refine this bias estimate in the HDO/H_2O ratio. We assume that the bias in the TES HDO data is due to uncertainties in the spectroscopic line strengths (e.g., Toth, 1999; Webster and Heymsfeld, 2003). The correction for this bias must therefore account for the sensitivity of the retrieval since a bias in the line strengths would be indistinguishable from an offset in the retrieved HDO or H_2O concentrations. For example, if the TES HDO estimate showed zero sensitivity then the estimate would return to the a priori constraint regardless of the spectroscopic uncertainties. For this reason we use the following form for the bias correction as discussed in J. Worden et al. (2007):

$$\ln(\boldsymbol{q}^{\mathrm{HDO}}_{\mathrm{corrected}}) = \ln(\boldsymbol{q}^{\mathrm{HDO}}_{\mathrm{original}}) - \mathbf{A}_{\mathrm{DD}}(\boldsymbol{\delta}_{\mathrm{bias}}) \quad (1)$$

where $\boldsymbol{q}^{\mathrm{HDO}}_{\mathrm{original}}$ is the volume mixing ratio of the HDO profile as provided in the product files, $\mathbf{A}_{\mathrm{DD}}$ is the averaging kernel matrix (also provided in the product files), and $\boldsymbol{\delta}_{\mathrm{bias}}$ is a column vector of the same length as $\boldsymbol{q}^{\mathrm{HDO}}_{\mathrm{original}}$ that contains the bias correction. Note that this correction is only applied to HDO and not to H_2O. In the subsequent sections, we estimate this bias term through comparisons of the TES HDO/H_2O estimates to the in situ data from the Picarro and LGR instruments.

Note that we do not distinguish between spectroscopic uncertainties in HDO or H_2O biases because we cannot distinguish between their effects on the ratio. Consequently, we aggregate this error into the HDO bias because the sensitivity of the HDO estimates will always overlap the sensitivity of the H_2O but the reverse is not necessarily true.

4 Indirect comparison of TES data to in situ data

An indirect method for comparing the TES data to the in situ data is to compare there respective δ-D versus H_2O distributions for a large number of observations. This makes use of the expectation that the free tropospheric water vapor observed by TES around Hawaii should, on average, have a similar moist process history as the water vapor observed in situ at Mauna Loa. Figure 2 shows distributions of δ-D versus H_2O using the in situ measurements from the corrected Picarro/LGR data and all TES data taken during October 2008 that were within 1000 km of Hawaii. Only data where the degrees-of-freedom for signal for HDO is larger than 0.5 is used. Then, the TES HDO profiles are corrected for biases of 0.02, 0.05, 0.07, and 0.09. After this bias correction is applied, a mass weighted column average is calculated for each HDO/H_2O profile using the pressure range between 825 hPa and 464 hPa. These column averages, using the bias, are then compared to the δ-D versus H_2O distributions from the Picarro/LGR in situ. Figure 2 shows comparisons of the in situ distribution to the TES data for bias correction of 0.05. What we can conclude from this comparison is that the TES HDO data should be corrected by at least 0.05 % in order for $\sim$98 % of the TES HDO/H_2O distribution to be within the in situ distribution. However a correction as high as 0.09 (not shown) is also possible. However, we cannot narrow the range of this bias estimate using only these distributions because they are representative of different parts of the PBL and free troposphere resulting from the TES vertical sensitivity and the diurnal variability of the PBL height. We next discuss a refinement of this bias estimate using the diurnal variability of the in situ data to construct profiles of the HDO/H_2O ratio in order to improve the comparison of the in situ data to the TES profile data.

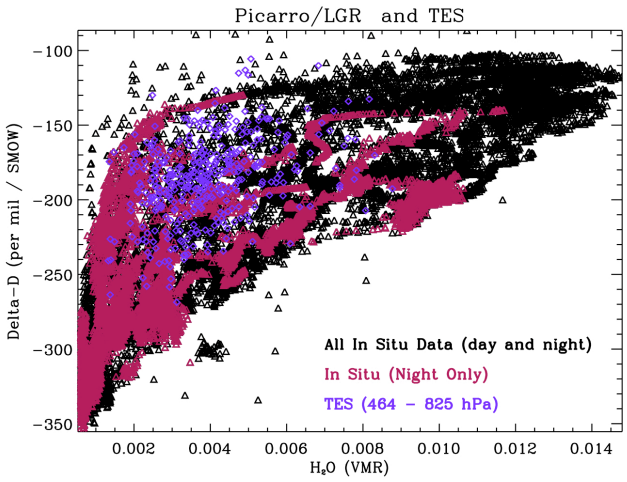

Fig. 2. (Black Diamonds) Distribution of δ-D versus H_2O from the average of the Picarro and LGR data from 11 October through 5 November 2008. (Red) Night-time values for these same data. (Blue) TES column averages for all data within 1000 km of Hawaii; the TES data have been corrected using a bias correction factor of 0.05, modified by the averaging kernel.

5 Direct comparison of TES satellite profile data to in situ data

We compare a TES profile measurement of the HDO/H_2O ratio to a constructed profile of the HDO/H_2O ratio using the Mauna Loa in situ data. Figure 1 shows strong diurnal variability in the HDO/H_2O ratio and in H_2O. During the day, values of the HDO/H_2O ratio are equivalent to PBL values but during the night they are representative of free tropospheric conditions. A profile of HDO and H_2O is constructed from these in situ measurements by mapping these daily variations to a pressure grid by comparing the in situ H_2O to the TES H_2O. Effectively, the vertical movement of the planetary boundary layer is used to construct a vertical profile of HDO and H_2O. The approach for this mapping is discussed in the next section (Sect. 5.1). Comparison of the in situ to the remotely sensed HDO/H_2O profile must also account for the sensitivity of the TES HDO/H_2O measurement to the true distribution of the HDO/H_2O ratio and to the a priori constraint used in the retrieval (e.g., Worden et al., 2006).

Once a profile is constructed, the comparison follows the approach described by H. M. Worden et al. (2007), for the TES ozone profiles except that we must account for the cross correlations in the joint HDO/H_2O profile retrieval used operationally by the TES algorithm, e.g.:

$$\hat{\boldsymbol{x}}_{\mathrm{R}} = x_{\mathrm{a}}^{\mathrm{R}} + (\mathbf{A}_{\mathrm{DD}} - \mathbf{A}_{\mathrm{HD}})(\boldsymbol{x}_{\mathrm{D}} - \boldsymbol{x}_{\mathrm{a}}^{\mathrm{D}}) - (\mathbf{A}_{\mathrm{HH}} - \mathbf{A}_{\mathrm{DH}})(\boldsymbol{x}_{\mathrm{H}} - \boldsymbol{x}_{\mathrm{a}}^{\mathrm{H}}) \quad (2)$$

Where, $\mathbf{A}_{\mathrm{DD}}$ and $\mathbf{A}_{\mathrm{HH}}$ are the averaging kernel matrices for HDO and H_2O separately (available in the individual product files for those species). The $\mathbf{A}_{\mathrm{HD}}$ and $\mathbf{A}_{\mathrm{DH}}$ are the cross averaging kernels between HDO and H_2O and the reverse; these matrices are available in the Ancillary product files. Note that the averaging kernels are not symmetric so one cannot use one cross term for the other. The $\boldsymbol{x}_{\mathrm{D}}$, $\boldsymbol{x}_{\mathrm{H}}$, are the "true" distribution of HDO and H_2O respectively and are represented as the log of the concentration of each species (given in volume mixing ratio), $\boldsymbol{x} = \log(\boldsymbol{q})$, where $\boldsymbol{q}$ is the volume mixing ratio of H_2O or HDO. The $\boldsymbol{x}_{\mathrm{a}}$ is the a priori constraint vector for each species (available in the product files). We have not included error terms related to interfering species or noise in Eq. (1); these error terms are discussed in Worden et al. (2006) and will be quantified in Sect. 5.3. For this analysis, the "true" HDO and H_2O values will be constructed from the in situ data shown in Fig. 1.

After passing the "true" HDO and H_2O and constraint vector profiles through the averaging kernels, the "true" HDO/H_2O ratio (or actually log[HDO/H_2O]), $\hat{\boldsymbol{x}}_{\mathrm{R}}$, will have been adjusted to account for the sensitivity of the TES estimate to HDO and H_2O and also to the bias introduced into the retrieval via the constraint vector that is used to regularize the retrieval; the error from this bias and vertical resolution is also called "smoothing error" (Rodgers, 2000). As shown in H. M. Worden et al. (2007) for the TES ozone retrievals, and in Worden et al. (2006) for the HDO/H_2O retrievals, the difference between this modified "true" ratio and the measurement from TES is due to uncertainties in the in situ data used to construct the true profile, any un-quantified biases in the TES data, as well as the measurement uncertainty due to noise and other geophysical parameters that affect the TES HDO/H_2O retrieval such as temperature, emissivity, and clouds:

$$\hat{\boldsymbol{x}}_{\mathrm{R}}^{\mathrm{TES}} - \hat{\boldsymbol{x}}_{\mathrm{R}}^{\mathrm{in\ situ}} = (\mathbf{A}_{\mathrm{DD}} - \mathbf{A}_{\mathrm{HD}})(\boldsymbol{e}_{\mathrm{D}}) - (\mathbf{A}_{\mathrm{HH}} - \mathbf{A}_{\mathrm{DH}})(\boldsymbol{e}_{\mathrm{H}}) + \mathbf{G}_{\mathrm{R}} n + \mathbf{G}_{\mathrm{R}} \sum_i \boldsymbol{K}_i^{\mathrm{b}} (\boldsymbol{b}_i - \boldsymbol{b}_i^{\mathrm{a}}) \quad (3)$$

where ε_{D} and ε_{H} are the uncertainties of the in situ HDO and H_2O concentrations respectively and the last two terms describe the uncertainties due to noise and other geophysical parameters (e.g., temperature and clouds) that affect the TES estimate. Following the approach in Worden et al. (2006) and H. M. Worden et al. (2007), specifically Eq. (23) through (27) in Worden et al. (2006), we can show that the statistics of this difference is described as follows:

$$\begin{aligned}\mathbf{S}_{\tilde{x}} &= E[(\hat{\boldsymbol{x}}_{\mathrm{R}}^{\mathrm{TES}} - \hat{\boldsymbol{x}}_{\mathrm{R}}^{\mathrm{in\ situ}})(\hat{\boldsymbol{x}}_{\mathrm{R}}^{\mathrm{TES}} - \hat{\boldsymbol{x}}_{\mathrm{R}}^{\mathrm{in\ situ}})^{\mathrm{T}}] \\ &= (\mathbf{A}_{\mathrm{DD}} - \mathbf{A}_{\mathrm{HD}})\mathbf{S}_{\mathrm{DD}}(\mathbf{A}_{\mathrm{DD}} - \mathbf{A}_{\mathrm{HD}})^{\mathrm{T}} \\ &+ (\mathbf{A}_{\mathrm{HH}} - \mathbf{A}_{\mathrm{DH}})\mathbf{S}_{\mathrm{HH}}(\mathbf{A}_{\mathrm{HH}} - \mathbf{A}_{\mathrm{DH}})^{\mathrm{T}} \\ &- (\mathbf{A}_{\mathrm{DD}} - \mathbf{A}_{\mathrm{HD}})\mathbf{S}_{\mathrm{DH}}(\mathbf{A}_{\mathrm{HH}} - \mathbf{A}_{\mathrm{DH}})^{\mathrm{T}} \\ &+ (\mathbf{A}_{\mathrm{HH}} - \mathbf{A}_{\mathrm{DH}})\mathbf{S}_{\mathrm{HD}}(\mathbf{A}_{\mathrm{DD}} - \mathbf{A}_{\mathrm{HD}})^{\mathrm{T}} \\ &+ \mathbf{G}_{\mathrm{R}}\mathbf{S}_n\mathbf{G}_{\mathrm{R}}^{\mathrm{T}} + \mathbf{G}_{\mathrm{R}}(\sum_i \mathbf{K}_i \mathbf{S}_{\mathrm{b}}^i \mathbf{K}_i^{\mathrm{T}})\mathbf{G}_{\mathrm{R}}^{\mathrm{T}} \end{aligned} \quad (4)$$

where as shown in Worden et al. (2006) : $\mathbf{S}_{\mathrm{DD}} = \mathbf{S}_{\mathrm{HH}} + \mathbf{S}_{\mathrm{R}}$, $\mathbf{S}_{\mathrm{DH}} = \mathbf{S}_{\mathrm{HD}} = \mathbf{S}_{\mathrm{HH}}$ and these covariances can be calculated as the expectation $E[]$ of the corresponding uncertainties: $\mathbf{S}_{\mathrm{DD}} = E[(\varepsilon_{\mathrm{D}})(\varepsilon_{\mathrm{D}})^T]$, $\mathbf{S}_{\mathrm{HH}} = E[(\varepsilon_{\mathrm{H}})(\varepsilon_{\mathrm{H}})^T]$, and

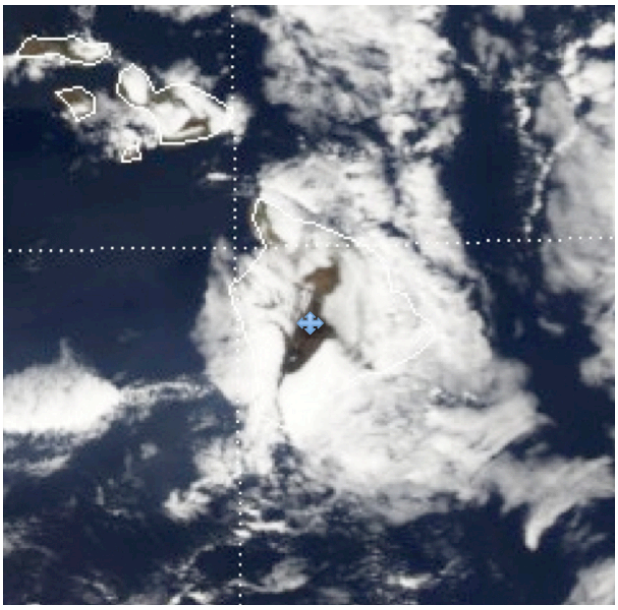

Fig. 3. MODIS clouds for 19 October 2008 23:45 UTC centered over the Big Island of Hawaii. The blue cross marks the approximate location of the Mauna Loa observatory.

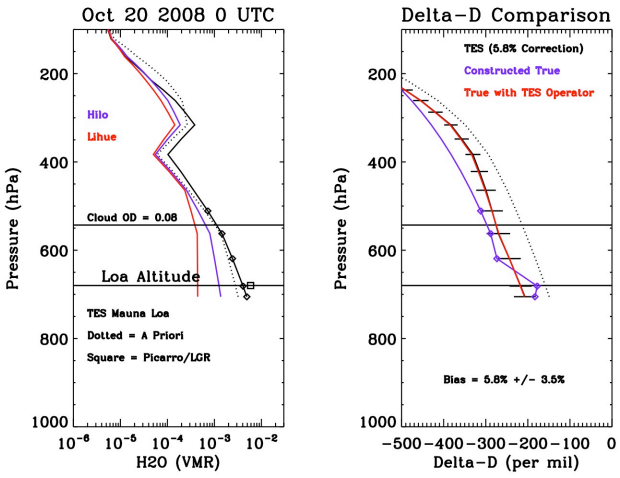

Fig. 4. (Left Panel) TES and sonde H_2O. The colored solid lines show H_2O measurements from sondes launched in Hilo and Lihue and modified by the TES H_2O averaging kernel and a priori constraint (dotted line). Right Panel: the TES δ-D profile (corrected for bias), the a priori constraint (dotted line), the constructed "true" δ-D profile (solid blue line), and the "true" profile modified by the TES averaging kernel and a priori constraint (solid red line). The error bars are due to measurement and interfering geophysical parameters as well as errors in the constructed "true" profile. The cloud top height is the solid line. Diamonds in both plots refer to the pressure levels used to construct the "true" δ-D profile. The square in the left panel is the corresponding in situ measurement at the time of the TES overpass.

$\mathbf{S}_R = E[(\varepsilon_R)(\varepsilon_R)^T]$. The last two terms are provided with the TES products. We next need to evaluate $\mathbf{S}_R$ and $\mathbf{S}_{HH}$ which are the uncertainties in the in situ values for the δ-D ratio and water values. These errors will depend on how the in situ data are used to create a profile of H_2O and the HDO/H_2O ratio as discussed next.

5.1 Comparison of in situ data to TES HDO/H_2O profiles

We next describe the approach for comparing the in situ data to the HDO/H_2O profiles. We only used those TES observations that were taken directly over the Mauna Loa observatory because we found that the variability in the H_2O and HDO/H_2O estimates for the 32 observations along the TES transect was larger than the expected error in the bias. To corroborate the reasons for this variability, Fig. 3 shows the cloud field over Mauna Loa, as measured by the Aqua Moderate Resolution Imaging Spectroradiometer (MODIS) instrument (e.g., Barnes et al., 1998), on 20 October 2008, approximately 02:00 p.m. local time. While most of the island is covered in clouds, the air directly above the Mauna Loa volcano and NOAA observatory are apparently cloud free; this information from the MODIS visible light measurement is consistent with the estimated cloud optical depth of 0.08 from the TES estimate directly over Mauna Loa. In addition, Fig. 4 (left panel) shows H_2O profiles from a nearby sonde launched from Hilo and also Lihue, approximately 500 km NW of Mauna Loa. The sonde data is downloaded from a U. of Wyoming resource (http://weather.uwyo.edu/upperair/sounding.html). The sondes are typically launched over the ocean and show humidity profiles that are much drier than that measured directly over Mauna Loa by TES, consistent with previous Lidar measurements of H_2O over Mauna Loa (Barnes et al., 2008). For this measurement, the bottom level of the TES H_2O profile is approximately 0.5 % (fraction of H_2O relative to total dry air amount) as compared to the in situ measurement of about 0.7 % (square symbol) for all in situ data taken within 1 h of the TES overpass. As can be seen in the left panel of Fig. 5, the TES H_2O estimate is most sensitive to the air directly above Mauna Loa (but not at the surface) and the total uncertainty (calculated from the total error covariance in the TES product files for this profile) for this estimate is approximately 7 %. As the bias in the TES lower tropospheric H_2O data is less than 5 % we would expect reasonable agreement between TES and the in situ data (Shepard et al., 2007). Differences of 0.2 % are likely because the TES and in situ measurements are not sampling exactly the same air parcels and because the variability in H_2O is high during this day as shown by the in situ measurements. For comparisons between the in situ data and TES it is important that the H_2O concentrations be "close" in order for the comparisons to be valid as we make use of δ-D/H_2O variations to calculate a "true" profile of δ-D as discussed

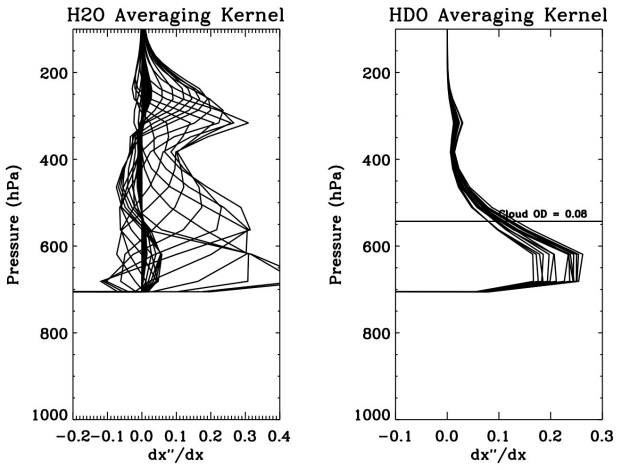

Fig. 5. The averaging kernels (rows of the averaging kernel matrix) for the H_2O and HDO components of the retrieval. The cloud top height is shown as a solid line (with cloud optical depth of 1.3) in the right panel.

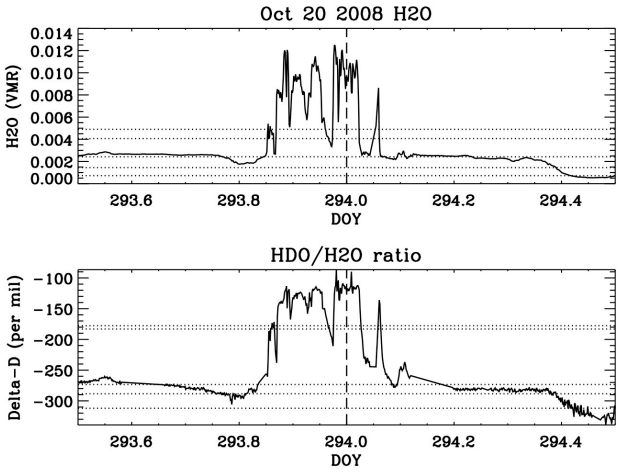

Fig. 6. H_2O (top) and δ-D (bottom) values derived from averaging the LGR and Picarro measurements. The horizontal dotted lines correspond to water values at the first five pressure levels of the TES H_2O profile shown in Fig. 3. The vertical dashed line corresponds to the time of the TES overpass.

in Sect. 5.2. In addition, the TES averaging kernels, used for accounting for the TES sensitivity to H_2O and HDO in comparisons between TES measurements and other data, are only valid if the estimated H_2O is close to the "true" H_2O We therefore conclude from the sonde and MODIS data that we should only use the TES measurements directly over Mauna Loa where the H_2O measurements best agree.

Only three daytime observations (out of five total direct TES observations) could be used for inter-comparison with the in situ data. These observations were taken on 20 and 22 October and 5 November 2008. Two night-time measurements could not be directly used because the sensitivity was too low due to cold temperatures and clouds. The quality checks of the three TES measurements showed that the three measurements had all converged to a reasonably solution as indicated primarily by comparing there radiance residuals and radiance residual mean relative to the TES noise levels. We next describe the approach for comparing the in situ data to the 20 October 2008 TES observation.

5.2 Construction of HDO/H_2O profile from in situ data

As noted earlier, the altitude variability of the boundary layer height is used to construct an altitude profile of the HDO/H_2O ratios for use in comparing to the estimated HDO/H_2O profile from TES, after accounting for the a priori constraint and vertical sensitivity as described in Eq. (2). We map the in situ H_2O and HDO data onto a vertical pressure grid using the H_2O values and pressure levels observed by TES during its over-flight. The set of in situ values which lie within 5 % (or 10 % if more matching pairs are needed) of an H_2O value observed by TES at a particular TES pressure level are averaged to give the constructed true values of H_2O and HDO at that level. The mapping approach is described next and the errors associated with this mapping are discussed in Sect. 5.3.

The following steps are used to construct each HDO/H_2O profile.

1. Obtain in situ HDO and H_2O data corresponding to the day of the satellite overpass. An example of these data from the Picarro/LGR average for 20 October is shown in Fig. 6. The time of the TES satellite overpass is shown as a vertical dashed line.

2. Identify where the TES H_2O data at each pressure level (diamonds in left panel of Fig. 4 and dotted lines in Fig. 6) matches to the in situ data. Note that in this instance only the first 5 pressure levels are used because H_2O amounts lower than 0.1 % were not measured by the Picarro and LGR instruments for this time period.

3. Average all δ-D values from the corrected Picarro/LGR data where the TES and in situ H_2O values agree to within 5 % for the 21 October and 5 November observations and 10 % for the 20 October observation; these δ-D values for the first five pressure levels correspond approximately to the dotted lines in the bottom of Fig. 6. After this step we have matching δ-D/pressure pairs that can be used to construct a δ-D profile. The 5 % and 10 % thresholds were chosen ad hoc to balance the number of corresponding in situ H_2O measurements that could be compared to the TES H_2O versus increasing the representation error by increasing the threshold. For the 5 % threshold there were between 30–90 matching pairs. The 10 % threshold was needed for the 20 October sounding to obtain at least 10 matching pairs. As

seen in the right panel of Fig. 5 these points span the altitude range where the TES HDO/H_2O estimates are most sensitive

4. Construct the δ-D profile using the matching H_2O values from Step 3; the lower troposphere values correspond to the TES pressure levels indicated by diamonds in Fig. 4. For the range of pressures (or altitudes) for which we do not have corresponding in situ and TES measurements of H_2O we interpolate between the in situ measurements (diamonds in Fig. 4) to the a priori constraint vector at 200 hPa.

5. Calculate the "true" HDO profile using the TES H_2O profile from the left panel in Fig. 4 and the "true" δ-D profile shown as the green line in the right panel of Fig. 4.

6. The last step involves transforming the HDO and H_2O profiles with the combined HDO/H_2O averaging kernel matrix using Eq. (2). The modified estimate for HDO and H_2O can now be compared to the TES estimate as it accounts for the TES sensitivity and a priori bias; this is shown as the red line in the right panel of Fig. 4.

5.3 Error characterization

The approach of using the diurnal variability of the HDO and H_2O concentrations to construct a vertical profile makes use of several assumptions; these assumptions will impart an error that must be accounted for in the comparison between the TES estimate and the profile constructed by the in situ data. These errors are propagated to the error covariances S_R and S_{HH} shown in Eq. (4). We next list the set of assumptions and the estimated errors associated with these assumptions.

1. *Pressure Grid Interpolation Error*
   for the three cases, TES measured H_2O concentrations range from approximately 1 % (relative to dry air) to 0.1 % over 300 hPa in pressure while there is a range of 150 ‰ for δ-D over similar pressures (Note that the ‰ unit can also be referred to as "per mil" and is parts per thousand relative to the isotopic composition of ocean waters or SMOW). The uncertainty in the TES H_2O is approximately 15 %. We calculate the error in the pressure grid to be:

   $200\,\text{hPa} \cdot 0.15/(\log(0.01)\text{–}\log(0.001) = 13\,\text{hPa}$.
   The corresponding uncertainty in δ-D is: $13\,\text{hPa} \cdot [150\,‰/300\,\text{hPa}] = 6.5‰$ which is small enough to ignore in this analysis.

2. *Use of TES H_2O for "true" H_2O in Pressure Grid interpolation*
   the error from this assumption propagates to the total error by replacing the covariance matrix, $\mathbf{S}_{HH}$, in Eq. (4) with the error covariance from the TES H_2O estimate, available in the TES product file. Although the uncertainties in the TES H_2O product range from 10 to 20 %, this uncertainty does not directly propagate into the ratio as a 10 % to 20 % uncertainty due to error cancellation as shown in Eq. (4) and Worden et al. (2006).

3. *Assumption that night-time air parcels are representative of day-time free troposphere*
   there are two ways in which this assumption could provide an incorrect assessment of the bias estimate: (a) if the actual daytime free-tropospheric δ-D values were biased high relative to night-time air with similar H_2O concentrations; this could happen because of mixing processes and (b) the variability of the night-time air for a range of H_2O values is larger than expected.

   Based on the results shown in Fig. 2 we conclude that the bias estimate must at least be 0.05 but with values up to 0.09 possible. Artificially increasing the night-time values used to estimate daytime free-tropospheric δ-D values by, for example, 50 ‰ would result in a decrease in our bias estimate from about 0.06 to less than 0.02 which is inconsistent with this result. In addition, much lower δ-D values for the night-time air would not be expected based on the distribution shown in Fig. 2. We therefore conclude that these night-time values of δ-D/H_2O pairs are reasonable estimates of similar daytime free tropospheric air for these observations.

   As discussed in Sect. 5.2 we address (b) by including night-time measurements that are before and after each daytime measurements; the variability in these measurements is the assumed uncertainty from this assumption of the corresponding δ-D/H_2O pairs used for comparison with the TES data. These uncertainties (or actually the square of these estimated uncertainties) are propagated into the error budget as the first five diagonal elements in the $\mathbf{S}_R$ matrix shown in Eq. (4). These uncertainties are shown, for example, in Fig. 7 as the diamonds which represent the square root of the diagonals of the $\mathbf{S}_R$ covariance matrix.

4. *Sensitivity of TES estimate from middle/upper troposphere on bias estimate*
   in order to conservatively account for this effect we replace the pressure levels in the $\mathbf{S}_R$ matrix that are not quantified with the in situ measurements with the a priori covariance matrix used for the TES retrievals and which describe the expected variability of δ-D in the free troposphere However, we multiply this a priori matrix by a factor of nine so that the variance in δ-D described by this matrix (square root of the diagonals)

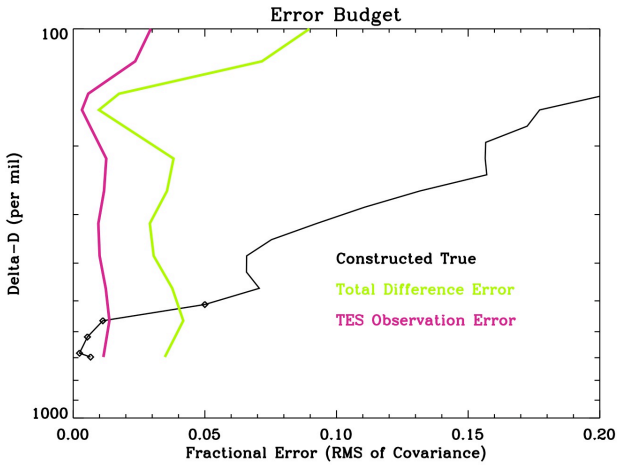

Fig. 7. Error budget for the TES and in situ data comparison for 20 October 2008. The diamonds are the pressure levels corresponding to in situ measurements. The black line is the total error for the constructed true profile. The red line is the observation error (noise + interfering species) for the TES estimate. The green line is the error in the difference between the TES estimate and the true profile after accounting for the TES sensitivity.

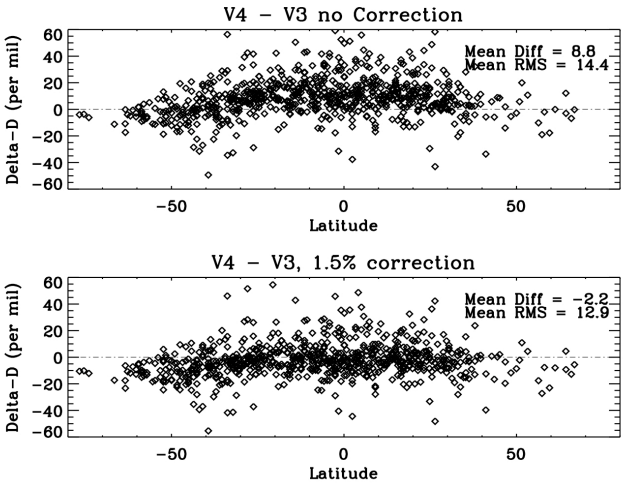

Fig. 8. Comparison between V4 and V3 of the TES HDO/H_2O ratios, averaged between 825 and 500 hPa. The bottom panel includes a 1.5 % correction to V4, modified by the HDO averaging kernel.

better agrees with the variance of the in situ data. This modification increases our error in the bias by approximately 1 %. The square root of the diagonal of this matrix is shown in Fig. 7 as the black line for pressure below 500 hPa.

The total error described by Eq. (4) can now be calculated after calculation of the full $\mathbf{S}_R$ matrix (black line in Fig. 7), substitution of the $\mathbf{S}_{HH}$ matrix with the corresponding total error covariance for the TES H_2O estimate, and addition of the TES observation error for the HDO/H_2O ratio that are due to noise and interference. The square root of the diagonals of this total error covariance is the green line in Fig. 7.

5.4 Summary of direct comparison between TES and in situ data

Bias estimates and their uncertainties are found by first averaging the lower tropospheric δ-D values (corresponding to the diamonds in Figs. 4 and 7) of the TES estimate and comparing it to a similar averaging of the constructed true profile after the "true" profile has been adjusted to account for the retrieval a priori constraint and sensitivity. We derive the bias through iterative comparison of differences between the averages with different bias values until a comparison is less than 0.3 ‰. The precision of this bias is calculated by applying this same mapping to the total difference error covariance described by Eq. (4). The average of the bias corrections for the three TES profiles used in the direct comparisons is 0.061; with the three bias estimates being 5.8 % ± 3.5 %, 6.5 % ± 3.8 %, and 6.6 % ± 2.7 %. Treating these uncertainties as random results in an estimated mean bias from these 3 measurements of 6.3 % ± 1.9 %. Note that the differences between these three bias corrections is well within the calculated random error which suggests that we are being too conservative with our error estimates.

6 Comparison between Version 4 and Version 3

In this section we compare δ-D values between Version 4 and Version 3 of the TES isotope data. A significant difference between these versions is that the temperature retrieval strategy was changed in order to obtain improved atmospheric temperatures. Because the spectral absorption lines for both HDO and H_2O are temperature sensitive, this change will impact the HDO and H_2O estimates. Although these changes are likely due to temperature we can partially correct for them using the same approach as described in Eq. (1). After correcting for a 1.5 percent bias between the versions, the mean difference between versions is reduced from 8.8 parts ‰ to −2.2 parts ‰, as shown in Fig. 8. Note that there is a residual latitudinal difference at higher latitudes because this correction cannot completely account for the differences in the two versions due to the differences in the temperature retrieval.

7 Summary

HDO/H_2O estimates from TES radiance measurements taken directly over the Mauna Loa observatory were compared to in situ data at the Mauna Loa observatory. We first indirectly compared the TES HDO/H_2O estimates by calculating averages of the HDO/H_2O ratio between 825 and 464 hPa from TES measurements within 1000 km of Mauna Loa during

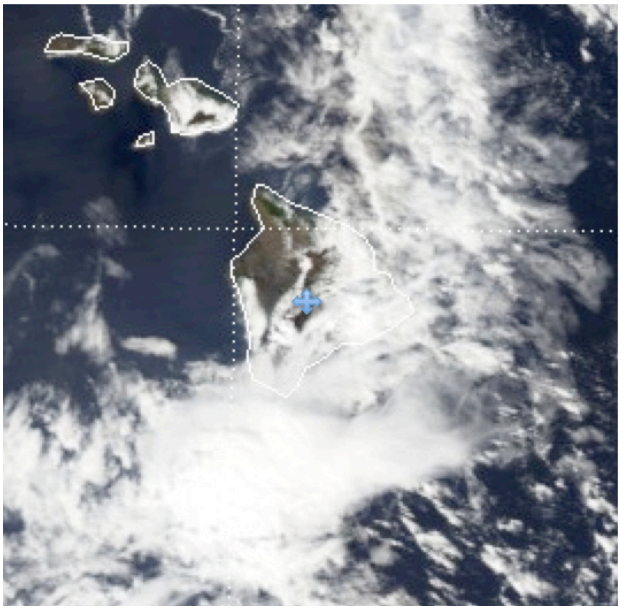

Fig. A1. Aqua MODIS image of the big island of Hawaii for 22 October approximately 00:00 UTC. The blue cross marks the approximate location of the observatory.

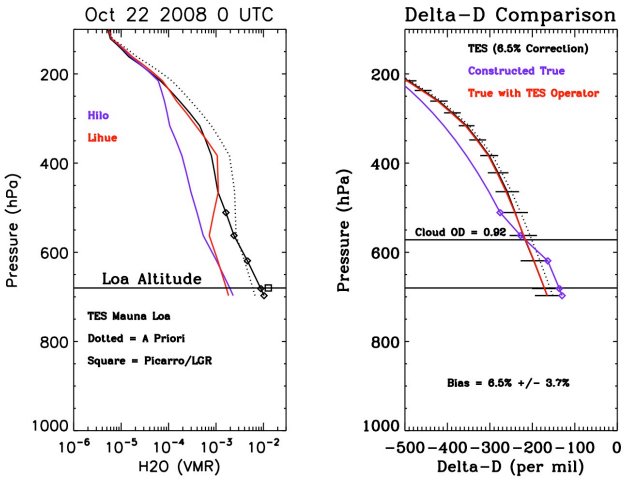

Fig. A2. (Left Panel) TES and sonde H_2O. The colored solid lines show H_2O measurements from sondes launched in Hilo and Lihue and modified by the TES H_2O averaging kernel and a priori constraint (dotted line). Right Panel: The TES δ-D profile (corrected for bias), the a priori constraint (dotted line), the constructed "true" δ-D profile (solid blue line), and the "true" profile modified by the TES averaging kernel and a priori constraint (solid red line). The error bars are due to measurement and interfering geophysical parameters as well as errors in the constructed "true" profile. The cloud top height is the solid line. Diamonds in both plots refer to the pressure levels used to construct the "true" δ-D profile. The square in the left panel is the corresponding in situ measurement at the time of the TES overpass.

this validation campaign and comparing them to the distribution of H_2O versus the HDO/H_2O ratio measured in situ at Mauna Loa. While the two distributions could not exactly be compared because of different contributions from the PBL and free troposphere we found that the TES HDO concentrations should be reduced by at least 5 % in order for the two distributions to be consistent. However, this comparison approach is not completely robust because greater reductions in the TES HDO could also be made and the two distributions would still be consistent. By using the vertical movement of the PBL during the day we could interpolate in situ measurements of H_2O and HDO to the TES pressure grid in the lower troposphere. This constructed altitude profile could then be compared to the TES estimates of HDO after accounting for the TES sensitivity and a priori constraint. The average of the bias corrections for the three TES profiles used in the direct comparisons is 0.061; with the three bias estimates being 5.8 % $\pm$ 3.5 %, 6.5 % $\pm$ 3.8 %, and 6.6 % $\pm$ 2.7 %. Treating these uncertainties as random results in a estimated mean bias from these 3 measurements of 6.3 % $\pm$ 1.9 %. Note that the differences between these three bias corrections is well within the calculated random error which suggests that we are being too conservative with our error estimates.

Finally, we compared Version 3 to Version 4 data and found that the Version 3 data should be bias corrected by 4.8 %. As with Version 4 data, this bias correction should not be directly applied to the HDO/H_2O ratio but instead be applied to the HDO profile and account for the TES HDO sensitivity and a priori constraint.

Appendix A

In this section we show comparisons between the 22 October and 5 November TES HDO/H_2O measurements and the corresponding in situ data. The figures shown in the Appendix correspond to Figs. 3 through 7 in the main text but for 22 October and 5 November respectively. As seen in Fig. A1 and Fig. A6 both measurements show significant cloud coverage and these visible light measurements are corroborated by the estimated cloud effective optical depth of 0.92 and 1.3 respectively and the estimated cloud top heights from TES as seen in Figs. A3 and A7. However the cloud optical depths are small enough such that the TES estimates are sensitive to the HDO/H_2O ratio below the cloud as seen in the averaging kernels for these observations (Figs. A4 and A8). These comparisons show that bias corrections of 6.5 % $\pm$ 3.8 %, and 6.6 % $\pm$ 2.7 % are required for agreement between the TES estimate and the in situ data.

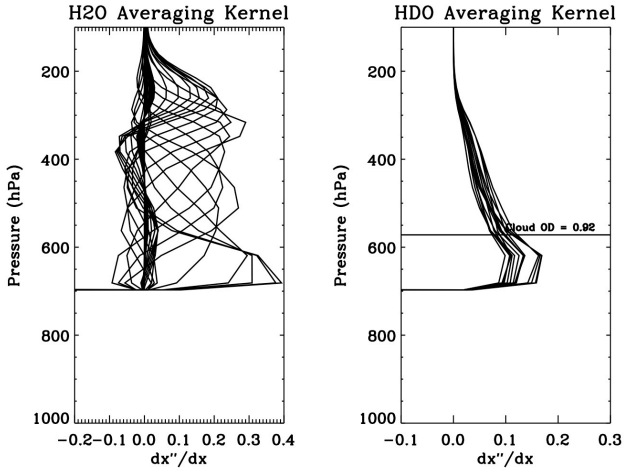

Fig. A3. (Left Panel) Averaging kernels for TES H_2O profile. (Right Panel) Averaging kernels for TES HDO profile. The cloud top height is shown as a solid in the right panel.

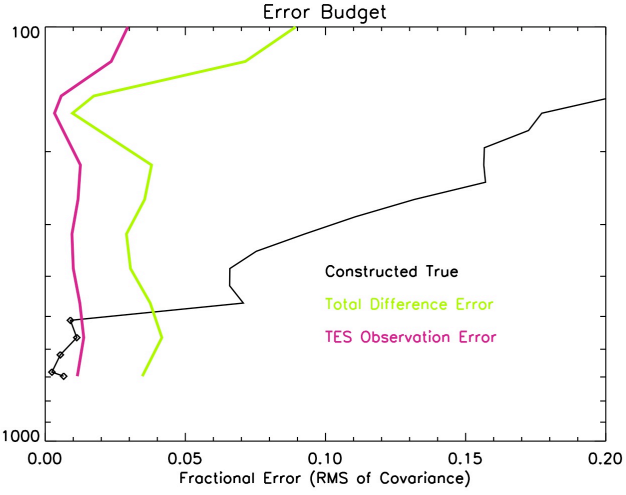

Fig. A5. Error budget for the TES and in situ data comparison for 22 October 2008. The diamonds are the pressure levels corresponding to in situ measurements. The black line is the total error for the constructed true profile. The red line is the observation error (noise + interfering species) for the TES estimate. The green line is the error in the difference between the TES estimate and the true profile after accounting for the TES sensitivity.

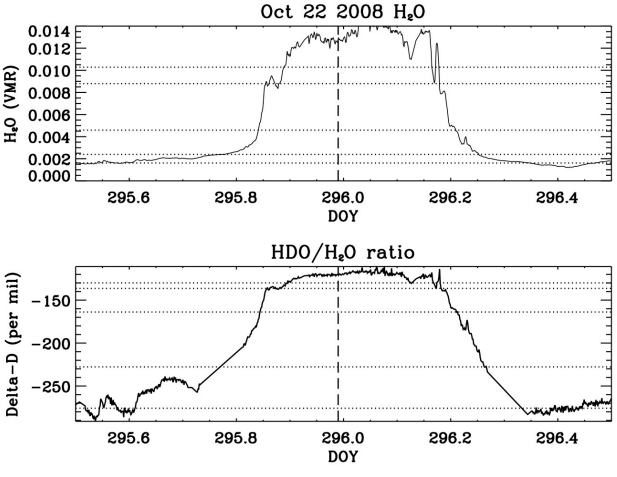

Fig. A4. Solid lines are the averaged values of the Picarro and LGR in situ measurements for H_2O (top) and δ-D (bottom). The horizontal dashed lines indicate the water and δ-D values used to construct the true HDO/H_2O profile. The vertical dashed line corresponds to the time of the TES overpass.

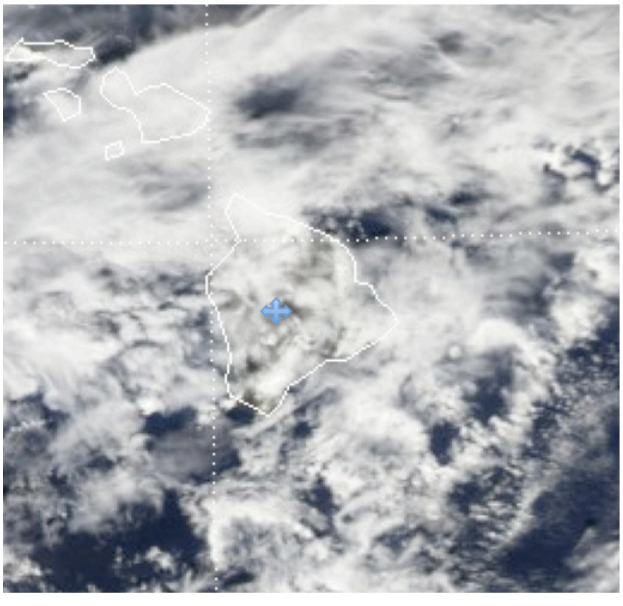

Fig. A6. Aqua MODIS image of the Hawaii islands for 5 November 2008 ~00:00 UTC. The big island is just south of 20° N. The blue cross marks the approximate location of the observatory.

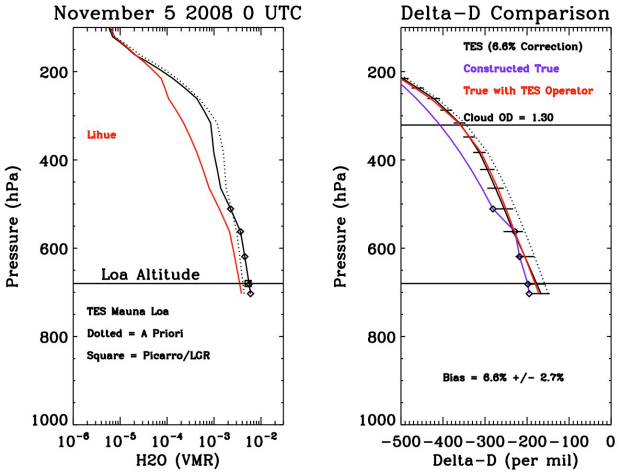

Fig. A7. Same as Fig. A2 but for 5 November 2008.

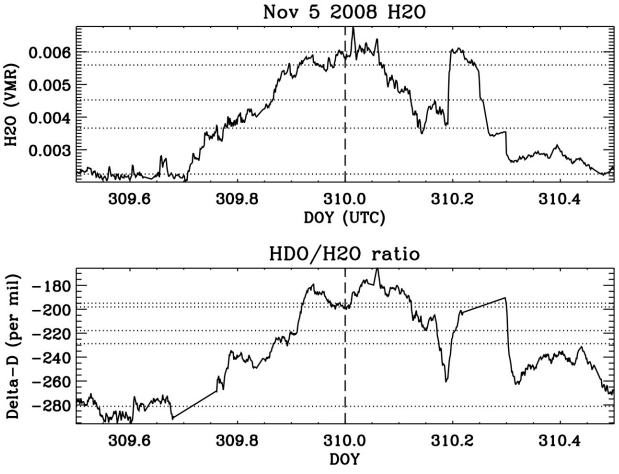

Fig. A9. Same as Fig. A4 but for 5 November 2008.

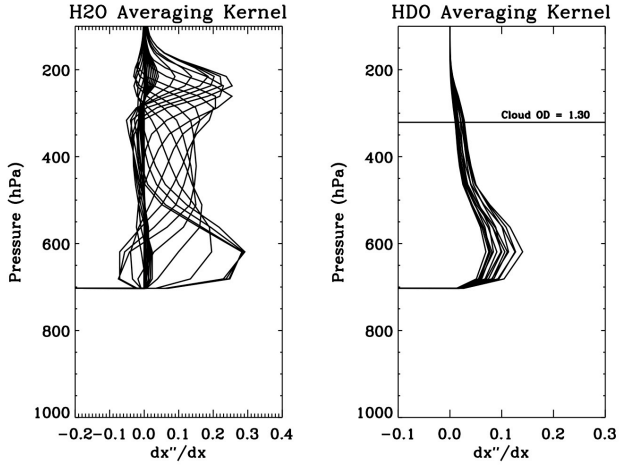

Fig. A8. Same as Fig. A3 but for 5 November 2008.

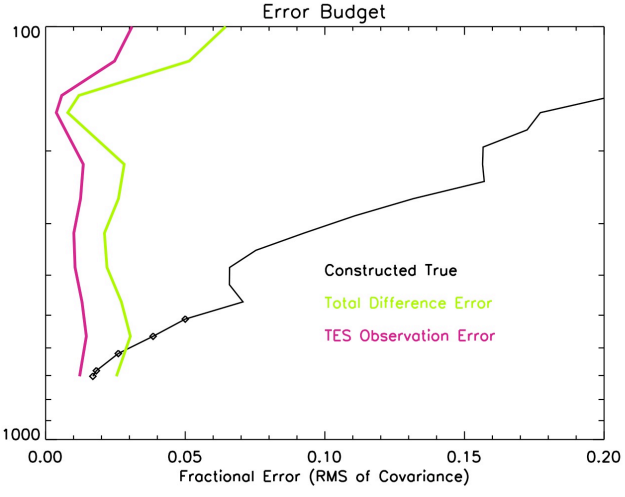

Fig. A10. Same as in Fig. A5 but for 5 November 2008.

Acknowledgements. We would like to thank Jung-Eun Lee and Christian Frankenberg for helpful comments. The work described here is performed at the Jet Propulsion Laboratory, California Institute of Technology under contracts from the National Aeronautics and Space Administration. The NASA ROSES Aura Science Team NNH07ZDA001N-AST 07-AST07-0069 contributed to the support of the analysis. The Mauna Loa field program was supported by NSF Grants ATM-084018 to Joe Galewsky and ATM-0840129 to David Noone. The views, opinions, and findings contained in this report are those of the author(s) and should not be construed as an official National Oceanic and Atmospheric Administration or U.S. Government position, policy, or decision.

Edited by: T. Röckmann

References

Barnes, W. L., Pagano, T. S., and Salomonson, V. V.: Prelaunch characteristics of the Moderate Resolution Imaging Spectroradiometer (MODIS) on EOS-AM1, IEEE T. Geosci. Remote, 36, 1088–1100, 1998.

Barnes, J. E., Kaplan, T., Vömel, H., and Read, W. G.: NASA/Aura/Microwave Limb Sounder water vapor validation at Mauna Loa Observatory by Raman lidar, J. Geophys. Res., 113, D15S03, doi:10.1029/2007JD008842, 2008.

Beer, R., Glavich, T. A., and Rider, D. M.: Tropospheric emission spectrometer for the Earth Observing System's Aura Satellite, Appl. Optics, 40, 2356–2367, 2001.

Boxe, C. S., Worden, J. R., Bowman, K. W., Kulawik, S. S., Neu, J. L., Ford, W. C., Osterman, G. B., Herman, R. L., Eldering, A., Tarasick, D. W., Thompson, A. M., Doughty, D. C., Hoffmann, M. R., and Oltmans, S. J.: Validation of northern latitude Tropospheric Emission Spectrometer stare ozone profiles with ARC-IONS sondes during ARCTAS: sensitivity, bias and error analysis, Atmos. Chem. Phys., 10, 9901–9914, doi:10.5194/acp-10-9901-2010, 2010.

Brown D., Worden, J., and Noone, D.: Comparison of atmospheric hydrology over convective continental regions using water vapor isotope measurements from space, J. Geophys. Res.-Atmos., 113, D15124, doi:10.1029/2007JD009676, 2008.

Craig, H.: Isotopic Variations in Meteoric Waters, Science, 133, 1702–1703 doi:10.1126/science.133.3465.1702, 1961.

Dansgaard, W.: Stable Isotopes in Precipitation, Tellus, 16, 436–468, 1964.

Frankenberg, C., Yoshimura, K., Warneke, T., Aben, I., Butz, A., Deutscher, N., Griffith, D., Hase, F., Notholt, J., Schneider, M., Schrijver, H., and T. Röckmann: Dynamic Processes Governing Lower-Tropospheric HDO/H_2O Ratios as Observed from Space and Ground, Science, 325, 1374–1377, 2009.

Galewsky, J., Strong, M., and Sharp, Z.: Measurements of water vapor D/H ratios from Mauna Kea, Hawaii, and implications for subtropical humidity dynamics, Geophys. Res. Lett., 34, L22808, doi:10.1029/2007GL031330, 2007.

Gupta, P., Noone, D., Galewsky, J., Sweeny, C., and Vaughn, B. H.: 2009: Demonstration of high precision continuous measurements of water vapor isotopologues in laboratory and remote field deployments using WS-CRDS technology, Rapid Communications in Mass-spectrometry, 23(16), 2534–2542, doi:10.1002/rcm.4100, 2009.

Herbin, H., Hurtmans, D., Turquety, S., Wespes, C., Barret, B., Hadji-Lazaro, J., Clerbaux, C., and Coheur, P.-F.: Global distributions of water vapour isotopologues retrieved from IMG/ADEOS data, Atmos. Chem. Phys., 7, 3957–3968, doi:10.5194/acp-7-3957-2007, 2007.

Herbin, H., Hurtmans, D., Clerbaux, C., Clarisse, L., and Coheur, P.-F.: $H_2{}^{16}O$ and HDO measurements with IASI/MetOp, Atmos. Chem. Phys., 9, 9433–9447, doi:10.5194/acp-9-9433-2009, 2009.

Johnson, L. R., Sharp, Z., Galewsky, J., Strong, M., Gupta, P., Baer, D., and Noone, D.: Hydrogen isotope measurements of water vapor and a correction for laser instrument measurement bias at low water vapor concentrations: applications to measurements from Mauna Loa Observatory, Hawaii, Rapid Communications In Mass Spectrometry, 25(5), 608–616, 2011.

Kuang, Z. M., Toon, G. C., Wennberg, P. O., and Yung, Y. L.: Measured HDO/H_2O ratios across the tropical tropopause, Geophys. Res. Lett., 30, 1372, doi:10.1029/2003GL017023, 2003.

Lee, J. E., Pierrehumbert, R., Swann, A., and Lintner, B. R.: Sensitivity of stable water isotopic values to convective parameterization schemes, Geophys. Res. Lett., 36, L23801, doi:10.1029/2009GL040880, 2009.

Lis, G., Wassenaar, L. I., and Hendry, M. J.: High-precision laser spectroscopy D/H and O-18/O-16 measurements of microliter natural water samples, Anal. Chem., 80, 287–293, 2008.

Moyer, E. J., Irion, F. W., Yung, Y. L., and Gunson, M. R.: ATMOS stratospheric deuterated water and implications for troposphere-stratosphere transport, Geophys. Res. Lett., 23, 2385–2388, 1996.

Nassar, R., Bernath, P. F., Boone, C. D., Gettelman, A., McLeod, S. D., and Rinsland, C. P.: Variability in HDO/H_2O abundance ratios in the tropical tropopause layer, J. Geophys. Res.-Atmos., 112, D21305, doi:10.1029/2007JD008417, 2007.

Payne, V. H., Noone, D., Piccolo, C., Grainger, R. G., and Dudhia, A.: Global satellite measurements of HDO and implications for understanding the transport of water vapour into the stratosphere, Q. J. Roy. Meteorol. Soc., 133, 1459–1471, 2007.

Risi, C., Bony, S., and Vimeux, F.: Influence of convective processes on the isotopic composition (delta O-18 and delta D) of precipitation and water vapor in the tropics: 2. Physical interpretation of the amount effect, J. Geophys. Res.-Atmos., 113, D19306, doi:10.1029/2008JD009943, 2008.

Rodgers, C. D.: Inverse Methods for Atmospheric Sounding: Theory and Practice, World Sci., Tokyo, 2000.

Schneider, M., Hase, F., and Blumenstock, T.: Ground-based remote sensing of HDO/H_2O ratio profiles: introduction and validation of an innovative retrieval approach, Atmos. Chem. Phys., 6, 4705–4722, doi:10.5194/acp-6-4705-2006, 2006.

Shephard, M. W., Herman, R. L., Fisher, B. M., Cady-Pereira, K. E., Clough, S. A., Payne, V. H., Whiteman, D. N., Comer, J. P., Vömel, H., Miloshevich, L. M., Forno, R., Adam, M., Osterman, G. B., Eldering, A., Worden, J. R., Brown, L. R., Worden, H. M., Kulawik, S. S., Rider, D. M., Goldman, A., Beer, R., Bowman, K. W., Rodgers, C. D., Luo, M., Rinsland, C. P., Lampel, M., and Gunson, M. R.: Comparison of Tropospheric Emission Spectrometer Nadir Water Vapor Retrievals with In Situ Measurements, J. Geophys. Res., 113, D15S24, doi:10.1029/2007JD008822, 2008.

Steinwagner, J., Fueglistaler, S., Stiller, G., von Clarmann, T.,

Kiefer, M., Borsboom, P.-P., van Delden, A., and Röckmann, T.: Tropical dehydration processes constrained by the seasonality of stratospheric deuterated water, Nature Geosci., 3, 262–266, 2010.

Toth, R. A.: HDO and D2O low pressure, long path spectra in the 600-3100 cm(-1) region I. HDO line positions and strengths, J. Molecular Spectrosc., 195, 73–97, 1999.

Webster, C. R. and Heymsfield, A. J.: Water isotope ratios D/H, O-18/O-16, O-17/O-16 in and out of clouds map dehydration pathways, Science, 302, 1742–1745, 2003.

Worden, H. M., Logan, J., Worden, J. R., Beer, R., Bowman, K., Clough, S. A., Eldering, A., Fisher, B., Gunson, M. R., Herman, R. L., Kulawik, S. S., Lampel, M. C., Luo, M., Megretskaia, I. A., Osterman, G. B., and Shephard, M. W.: Comparisons of Tropospheric Emission Spectrometer (TES) ozone profiles to ozonesondes: Methods and initial results, J. Geophys. Res., 112, D03309, doi:10.1029/2006JD007258, 2007.

Worden, J., Bowman, K., Noone, D., Beer, R., Clough, S., Eldering, A., Fisher, B., Goldman, A., Gunson, M., Herman, R., Kulawik, S., Lampel, M., Luo, M., Osterman, G., Rinsland, C., Rodgers, C., Sander, S., Shephard, M., and Worden, H.: Tropospheric Emission Spectrometer observations of the tropospheric HDO/H_2O ratio: Estimation approach and characterization, J. Geophys. Res., 111, D16309, doi:10.1029/2005JD006606, 2006.

Worden, J., Noone, D., Bowman, K., and TES science team and data contributors: Importance of rain evaporation and continental convection in the tropical water cycle, Nature, 445, 528–532, doi:10.1038/nature05508, 2007.

Zakharov, V. I., Imasu, R., Gribanov, K. G., Hoffmann, G., and Jouzel, J.: Latitudinal distribution of the deuterium to hydrogen ratio in the atmospheric water vapor retrieved from IMG/ADEOS data, Geophys. Res. Lett., 31, L12104, doi:10.1029/2004GL019433, 2004.